ZAMM-Journal of Applied Mathematics and Mechanics/
Zeitschrift für Angewandte Mathematik und Mechanik
https://onlinelibrary.wiley.com/journal/15214001
Impact factor:1.603

Accepted April 2nd 2023

Mixed convection Casson polymeric flow from a nonlinear stretching surface with radiative flux and non-Fourier thermal relaxation effects: Computation with CSNIS

A. Shahid[1], W. Wei[1], M. M. Bhatti[2,3*], O. Anwar Bég[4] and Tasveer A. Bég[5]

[1]*School of Science, Zhejiang University of Science and Technology, Hangzhou, 310023, P.R.* ***China.***
[2]*College of Mathematics and Systems Science, Shandong University of Science & Technology, Qingdao 266590, Shandong, P.R.* ***China.***
[3]*Material Science, Innovation and Modelling (MaSIM) Research Focus Area, North-West University, Mafikeng Campus, Private Bag X2046, Mmabatho 2735,* ***South Africa.***
[4] *Multi-Physical Engineering Sciences Group, Mechanical Engineering, Corrosion and Multiphysics Lab, SEE Building, Room 3-08, Salford University, Manchester, M54WT,* ***UK.***
[5] *Engineering Mechanics Research, Israfil House, Dickenson Rd., Manchester, M13,* ***UK****.*

Abstract:

Thermal non-Newtonian polymer coating flows is growing as a major area in materials processing. Inspired by new developments in this field which require more sophisticated mathematical models, the current investigation examines the laminar viscoplastic boundary layer flow and mixed convective heat transfer over a power-law nonlinear stretching surface. To simulate thermal relaxation effects the hyperbolic Cattaneo-Christov heat flux model is deployed. The non-Newtonian polymer characteristics are described by employing the Casson flow model. High temperature conditions invoke thermal radiation flux which is analyzed with an algebraic flux model. Via robust similarity transformations, the primitive partial differential conservation equations for momentum and energy equations are rendered into a system of coupled non-linear ordinary differential equations with associated wall and free stream boundary conditions. The emerging boundary value problem is solved numerically with an efficient Chebyshev Spectral Newton Iterative scheme (CSNIS), in the MATLAB platform. The resulting solutions are discussed for different emerging parameters using graphs and tables. Validation is included with special cases from the literature. With increasing power law stretching index increases, the flow

*Corresponding author: mmbhatti@sdust.edu.cn; mubashirme@yahoo.com

is decelerated, and temperatures are reduced. Increment in mixed convection parameter boosts the velocity but suppresses temperature and thermal boundary layer thickness. Increasing non-Fourier Deborah number, temperatures are depleted whereas with increasing radiative flux parameter they are increased. With elevation in Casson non-Newtonian parameter, velocity is decreased whereas temperature is enhanced and Nusselt number is suppressed.

Keywords: *Cattaneo-Christov heat flux; Mixed convection; thermal radiation; nonlinear stretching surface; non-Fourier; Chebyshev Spectral Newton Iterative Scheme; polymer coating.*

Nomenclature

$\overline{y}, \overline{x}$	Cartesian coordinates
c	Constant
U	Nonlinear stretching velocity
T_w	Temperature at the sheet surface (wall)
T_∞	Ambient (free stream) temperature
$\hat{u}, \hat{v}$	Velocity components
k^*	Rosseland mean spectral absorption coefficient
c_p	Specific heat
Gr	Grashof number
Pr	Prandtl number
Greek symbols	
λ	mixed convection parameter
ξ	Power index associated with surface stretching velocity
$\pi = e_{jk} e_{jk}$	Ratio between the deformed part with itself
π_c	Critical value of the Casson model
μ_D	Plastic dynamical viscosity
ς	Yield stress of liquid
$\beta_1 = \mu_D \sqrt{2\pi_c} \big/ \varsigma$	Casson viscoplastic parameter
$\overline{\sigma}$	Stefan-Boltzmann constant
κ	Thermal diffusivity of the polymer
ρ	Polymer fluid density
λ_2	Non-Fourier heat flux relaxation time
ν	Kinematic viscosity
γ	Modified Deborah number
$\Re$	Reynolds number

ζ	Radiation parameter

1. Introduction

Non-Newtonian fluids flowing over nonlinear stretching surfaces have stimulated the attention of scientists in recent years, due to advances in modern polymer materials processing systems and thermal coating deposition with viscoplastic materials. For instance, if a non-Newtonian liquid is used as the cooling and heating medium, the required injecting power may be greatly decreased. As a result, the analysis of non-Newtonian boundary layer flows adjacent to an elongating sheet is crucial in optimizing coating flows and in other technologies including heat exchange [1-3]. Many synthetic and natural liquids exhibit a range of non-Newtonian characteristics including slurries, muds, solidified milk, pastes, imprinting ink, amalgamations, cleansers, sugar suspensions, shampoos and thermoplastics. Non-Newtonian liquids have various features that differ from Newtonian liquids. These characteristics include viscoplasticity (yield stress behaviour), viscoelasticity, internal microstructure (couple stresses for example), relaxation, retardation, spurting and swelling. Non-Newtonian constitutive models are therefore more complex and generally non-linear when compared to the classic Newtonian model. Due to these complexities, there is no single constitutive equation that encompasses all of their features [4]. Therefore, a range of non-Newtonian models have been deployed in recent years to address various flow problems. In thermal polymer coating dynamics [5], heat is critical and *convective heat transfer* must also be simulated in addition to thermal conduction (at the wall) and thermal radiation for high temperature fabrication systems. The convective heat from stretching sheets with different non-Newtonian models has received considerable attention in the mathematical modelling community. Prakash *et al*. [7] used a tangent hyperbolic non-Newtonian nanofluid model to study biaxial stretching of electromagnetic polymers with convective and radiative heat transfer. Kumar *et al.* [8] deployed a differential transform method to compute the time-dependent convective boundary layer flow of a Stokes polar (couple stress) rheological fluid from a stretching sheet. Kumar *et al.* [8] explored the effects of thermal radiation and magnetic field on micropolar fluid moving from a stretching sheet with wall slip effects. Kumar *et al.* [9] analyzed the impact of radiative flux on non-aligned stagnation-point flow of a magnetized micropolar fluid from a convectively heated surface. Megahed [10] used the Sisko viscolastic model to compute the dissipative thermal convection boundary layer flow from a nonlinear extending surface with heat generation. Many other studies have been reported for non-Newtonian thermal flows from stretching surfaces in which linear, quadratic, exponential stretching velocity models have been deployed.

The above studies were restricted to the classical *Fourier model* for thermal conduction. This is a *parabolic* model and neglects thermal relaxation effects which can be significant in polymer processing. To more accurately represent thermal behaviour therefore a *non-Fourier*

model [11] is required. The Cattaneo-Christov model [12, 13] provides an excellent approximation for computing thermal relaxation effects associated with *hyperbolic heat conduction*. It has therefore been extensively explored in recent years in the context of polymer processing. Kumaran *et al.* [14] used the Keller box finite difference technique to compute the enrobing boundary layer flow of a rheological magnetized bio-nanofluid with the tangent hyperbolic model on a stretching cylinder with non-Fourier heat flux effects. They observed that temperature distributions deviate strongly from the Fourier case and that velocity and concentration fields are also modified substantially. Shahid *et al.* [15] deployed the Maxwell viscoelastic model to study non-Foruier heat flux effects on stretching sheet dynamics with radiative heat transfer and wall transpiration effects. Alhowaity *et al.* [16] considered the pseudoplastic nanofluid transport from a stretching surface with non-Fourier heat flux effects, noting a considerable modification in Nusselt number with stronger thermal relaxation. Mehmood *et al.* [17] applied both Runge–Kutta–Fehlberg numerical quadrature and Adomian decomposition methods to compute the non-orthogonal stagnation flow of a magnetized Oldroyd-B viscoelastic polymer on a stretching sheet with hetegrogenous chemical reaction and Cattaneo-Christov heat flux. They noted that thermal boundary layer thickness was reduced with stronger non-Fourier Deborah number and that wall shear stress was strongly modified. Sui *et al*. [18] employed the homotopy analysis method (HAM) to compute the non-Fourier thermo-solutal boundary layer heat and mass transfer of a Maxwell viscoelastic nanofluid from a stretching plane with hydrodynamic wall slip. They reported substantial reduction in the temperature magnitudes with enhanced thermal relaxation (Cattaneo-Christov) parameter. Han *et al.* [19] analyzed the Cattaneo-Christov heat flux effects on Maxwell fluid flow from a stretching surface. Mustafa [20] derived power series solutions for non-Fourier heat flux effects on rotating thermal convection flow of a Maxwell fluid. Many other studies have also been communicated of relevance to thermal polymer processing featuring non-Fourier heat flux models including Kumar *et al.* [21] (on wedge/cone external boundary layer flows), Saqlain *et al.* [22] (on mixed convection), Bhatti *et al.* [23] (on quadratic convection in Maxwell viscoelastic flows) and Mishra *et al*. [24] (on Von Karman swirling flows). Very recently Ray *et al.* [25] studied Eyring-Powell rheological polymer nanofluid flow from a stretching surface with with non-Fourier thermal relaxation effects. They showed that skin friction factor decreases with increasing Deborah (viscoelastic) number and also Cattaneo–Christov thermal relaxation parameter. All these studies have confirmed the substantial influence of non-Fourier heat flux in polymeric coating flow dynamics.

In the present article, a mathematical model is developed for *radiative mixed convective Casson viscoplastic polymer boundary layer flow from a nonlinear stretching sheet with Cattaneo–Christov thermal relaxation effects*. Thermal buoyancy effects are included. The Casson model provides an accurate description for real polymers and other suspensions deployed in coatings [26, 27]. The Casson model is a shear thinning model which is assumed to have an infinite viscosity at zero rate of shear, a yield stress below which no flow occurs, and a zero viscosity at an infinite rate of

shear, i.e., if a shear stress below the yield stress is applied to the polymer, it behaves like a solid, whereas if a shear stress greater than yield stress is applied, it starts to move [28, 29]. The current analysis also generalizes previous studies which considered only linear sheet stretching to consider general *power-law stretching rates* (quadratic, exponential etc) which provide a more robust representation of polymer coating flows. The Rosseland algebraic flux model is deployed to compute radiative flux effects [30, 31] since radiation is known to encourage cross-linking and enhance stability of optically dense polymers [32]. The transformed nonlinear ordinary differential boundary value problem is solved with an efficient, stable and rapidly converging Chebyshev Spectral Newton Iterative Scheme (CSNIS) [33]. There are different numerical methods (see refs. [34-38]) that can be used to solve such kind of problems, but the used numerical method has advantages over other numerical methods. In the proposed technique, we transform the domain of the proposed problem to [-1,1]. Further, we discretize this domain into few numbers of grid points, while employing some other numerical methods. To obtain the accuracy, we discretize the domain in thousands of points. Validation with special cases from the literature is included. Graphical plots are presented for the impact of key emerging parameter on velocity and temperature distributions. Nusselt number and skin friction are also computed in Tables. The thermal and hydrodynamic characteristics are described in detail.

2. Mathematical model for viscoplastic non-Fourier stretching polymer flow

Laminar, incompressible, steady-state flow of non-Newtonian Casson polymeric fluid along a vertical stretching sheet is considered. The stream of extruding polymer flow issuing from a slit is constrained at $\bar{y} > 0$. From a fixed origin, two equivalent and opposite forces are exerted to stretch the sheet along the $\bar{x}$ -axis. The sheet is extended with a nonlinear stretching velocity $U = c\bar{x}^{\xi}$, where c is a constant and ξ represents the power index associated with surface stretching velocity. The boundary layer regime is depicted in **Fig. 1**. A uniform radiative flux is applied transverse to the sheet plane. The polymer is assumed to absorb or emit radiation but not scatter radiation [32] and Rosseland's diffusion flux approximation, valid for high optical thickness is therefore deployed. Furthermore, T_w is the constant temperature imposed at the sheet surface (wall) with a corresponding uniform ambient (free stream) temperature, T_∞ . The appropriate constitutive equations for an isotropic and incompressible Casson fluid (viscoplastic polymer) are:

$$\tau_{jk} = \begin{cases} 2\left(\mu_D + \dfrac{\varsigma}{\sqrt{2\pi}}\right)e_{jk}, \pi > \pi_c, \\ 2\left(\mu_D + \dfrac{\varsigma}{\sqrt{2\pi_c}}\right)e_{jk}, \pi < \pi_c, \end{cases} \tag{1}$$

Here π is the ratio between the deformed part with itself, $\pi = e_{jk}e_{jk}, e_{jk}$ is the (j,k)-th part of the deformation ratio, π_c the critical value of the Casson model, and μ_D the plastic dynamical viscosity and ς the yield stress of liquid.

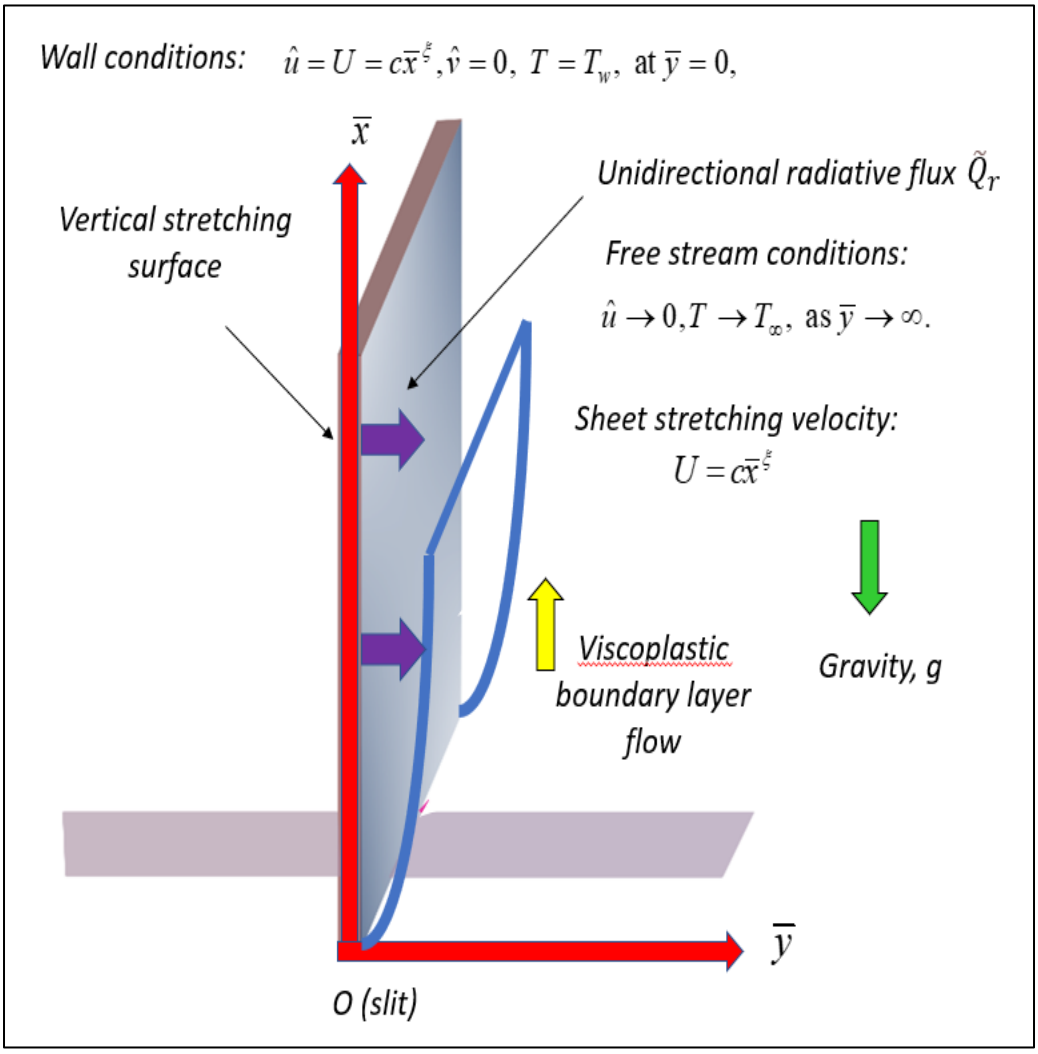

Fig. 1: Viscoplastic polymer stretching flow regime

Thermal buoyancy is invoked and under the Boussinesq approximation, the governing equations of continuity, momentum and energy conservation may be shown to assume the following form, extending earlier models [39, 40] to include *non-Fourier heat flux and non-Newtonian effects*:

$$\frac{\partial \hat{u}}{\partial \bar{x}} + \frac{\partial \hat{v}}{\partial \bar{y}} = 0, \tag{2}$$

$$\hat{u}\frac{\partial \hat{u}}{\partial \bar{x}}+\hat{v}\frac{\partial \hat{u}}{\partial \bar{y}}=\upsilon\left(1+\frac{1}{\beta_1}\right)\frac{\partial^2 \hat{u}}{\partial \bar{y}^2}+\bar{g}\beta\left(T-T_\infty\right), \tag{3}$$

$$\hat{u}\frac{\partial T}{\partial \bar{x}}+\hat{v}\frac{\partial T}{\partial \bar{y}}+\lambda_2\left[\begin{array}{l}\hat{u}\dfrac{\partial \hat{u}}{\partial \bar{x}}\dfrac{\partial T}{\partial \bar{x}}+\hat{v}\dfrac{\partial \hat{v}}{\partial \bar{y}}\dfrac{\partial T}{\partial \bar{y}}+\hat{u}\dfrac{\partial \hat{v}}{\partial \bar{x}}\dfrac{\partial T}{\partial \bar{y}}+\hat{v}\dfrac{\partial \hat{u}}{\partial \bar{y}}\dfrac{\partial T}{\partial \bar{x}} \\ +2\hat{u}\hat{v}\dfrac{\partial^2 T}{\partial \bar{x}\partial \bar{y}}+\hat{u}^2\dfrac{\partial^2 T}{\partial \bar{x}^2}+\hat{v}^2\dfrac{\partial^2 T}{\partial \bar{y}^2}\end{array}\right]=\kappa\frac{\partial^2 T}{\partial \bar{y}^2}-\frac{1}{\rho c_p}\frac{\partial \tilde{Q}_r}{\partial \bar{y}}. \tag{4}$$

The radiative flux (uni-directional) is expressed here as:

$$\tilde{Q}_r=-\frac{16\bar{\sigma}T_\infty^3}{3k^*}\frac{\partial T}{\partial \bar{y}}, \tag{5}$$

Where $\hat{u}$ and $\hat{v}$ denote velocity components in the $\bar{x}$ and $\bar{y}$ directions sequentially, $\beta_1=\mu_D\sqrt{2\pi_c}/\varsigma$ is the Casson viscoplastic parameter, $\bar{\sigma}$ the Stefan-Boltzmann constant, κ is the thermal diffusivity of the polymer, k^* is the Rosseland mean spectral absorption coefficient, ρ the polymer fluid density, λ_2 the non-Fourier heat flux relaxation time, ν is kinematic viscosity, and c_p the specific heat. The prescribed boundary conditions at the wall (sheet) and in the free stream are:

$$\hat{u}=U=c\bar{x}^{\xi},\hat{v}=0,\ T=T_w,\ \text{at}\ \bar{y}=0, \tag{6}$$

$$\hat{u}\to 0,T\to T_\infty,\ \text{as}\ \bar{y}\to\infty. \tag{7}$$

Invoking the following similarity transformations:

$$\left.\begin{array}{l}\hat{u}=c\bar{x}^{\xi}F'(\eta),\ \hat{v}=-\sqrt{\dfrac{\nu(\xi+1)c\bar{x}^{\xi-1}}{2}}\left[F(\eta)+\dfrac{\xi-1}{\xi+1}\eta F'(\eta)\right], \\ \eta=\bar{y}\sqrt{\dfrac{(\xi+1)c\bar{x}^{\xi-1}}{2\nu}},\ \theta=\dfrac{T-T_\infty}{T_w-T_\infty}.\end{array}\right\} \tag{8}$$

Using Eqn. (8) in Eqns. (2)-(7), generates the following non-dimensional boundary layer equations for momentum and energy (heat):

$$\left(1+\frac{1}{\beta_1}\right)F'''+FF''-\frac{2}{\xi+1}\left(\xi F'^2-\lambda\theta\right)=0, \tag{9}$$

$$\left(1+\frac{4}{3}\zeta\right)\theta''+\Pr F\theta'+\Pr\gamma\left(\frac{\xi-3}{2}FF'\theta'-\frac{\xi+1}{2}F^2\theta''\right)=0. \tag{10}$$

The associated transformed dimensionless boundary conditions are:

$$F(\eta)=0,\ F'(\eta)=\theta(\eta)=1,\ \text{at}\ \eta=0, \tag{11}$$

$$F'(\eta)=0,\ \theta(\eta)=0,\qquad \text{as}\ \eta\to\infty, \tag{12}$$

Here the following definitions apply:

$$\lambda = \frac{Gr}{\Re^2} = \frac{g\beta\left(T_w - T_\infty\right)\bar{x}^3/\nu^2}{U^2\bar{x}^2/\nu^2}, \Pr = \frac{\upsilon}{\kappa}, \zeta = \frac{4\bar{\sigma}T_\infty^{\ 3}}{k^*\kappa}, \gamma = \lambda_2 c\bar{x}^{\xi-1}. \tag{13}$$

where Gr the Grashof number, λ the mixed convection parameter, $\Pr$ the Prandtl number, γ the modified Deborah number featuring non-Fourier heat flux relaxation time, $\Re$ the Reynolds number and ζ the radiation parameter, respectively.

The dimensionless form of *skin friction* and *Nusselt number* with thermal radiative flux contribution (both of which are useful for assessing wall characteristics), take the form:

$$\left.\begin{aligned} \text{Skin friction} = Cf\,\Re^{1/2} &= \sqrt{\frac{n+1}{2}}\left(1+\frac{1}{\beta_1}\right)F''(0), \\ \text{Nusselt number} = Nu\,\Re^{-1/2} &= -\sqrt{\frac{n+1}{2}}\left(1+\frac{4}{3}\zeta\right)\theta'(0). \end{aligned}\right\} \tag{14}$$

3. Numerical Method: *The CSNIS Technique*

Accurate (exact) solutions of the non-linear differential Eqs. (9)-(10) subject to the boundary conditions (11)-(12) are extremely difficult if not intractable, due to the non-linearity. A few investigators have utilized scientific semi-analytical methods similar equations. In the current investigation, we utilized a numerical approach known as CSNIS (Chebyshev Spectral Newton Iterative Scheme). This method has been applied in a range of materials processing applications in recent years including slip flow on stretching cylinders [41] and boundary layer flows [42]. Firstly, the Newton iterative scheme is employed to transmute the collection of nonlinear ordinary differential equations into a linear system. We can write for $(j+1)^{th}$ iterations:

$$F_{j+1} = F_j + \delta F_j, \ \theta_{j+1} = \theta_j + \delta\theta_j, \tag{15}$$

This applies for every dependent variable, where δF_j, $\delta\theta_j$, presents a smaller change in F_j, and θ_j, separately. The Eqns. (9)- (12) in a linearized form are:

$$\left.\begin{aligned} &\left(1+\frac{1}{\beta_1}\right)\delta F_j''' + \mathrm{A}_{1,j}\,\delta F_j'' + \mathrm{A}_{2,j}\,\delta F_j' + \mathrm{A}_{3,j}\,\delta F_j + \frac{2}{\xi+1}\lambda\theta_j = R_{1,j}, \\ &\left(1+\frac{4}{3}\zeta\right)\delta\theta_j'' + B_{1,j}\delta\theta' + \mathrm{B}_{2,j}\,\delta\theta' + \mathrm{B}_{3,j}\,\theta_j'' = R_{2,j}. \end{aligned}\right\} \tag{16}$$

The corresponding boundary conditions emerge as:

$$\delta F_j(0) = -F_j(0),\ \delta F_j'(0) = 1 - F_j'(0),\ \delta\theta_j(0) = 1 - \theta_j(0), \tag{17}$$

$$\delta F_j'(\infty) = 0 - F_j'(\infty),\ \delta\theta_j(\infty) = 0 - \theta_j(\infty). \tag{18}$$

Secondly, the new set of linearized Eqns. (16) dependent upon boundary conditions (17)-(18) is solved utilizing the Chebyshev spectral collocation technique [42]. Accordingly, the actual domain [0, ∞) is transformed to finite domain [0, *L*]. The converted area is changed to [-1, 1] by utilizing the transformation, $\bar{\xi} = 2\eta / L - 1$, and the nodal points from -1 up to 1 are specified as Gauss-Lobatto collocation points using $\zeta_k = \cos(\pi_k / N),\ k = 0,1,2,...,N,$. The CSNIS depends on the differentiation matrix [D], and it can be approximated using a process very similar to that proposed by Trefethen [43]. In Eqn. (16), the coefficients $\mathrm{A}_{i,j}$, $B_{i,j}$, $R_{i,j}$, $i = 1,2,.....$ are:

$$\left.\begin{aligned}
&\mathrm{A}_{1,j} = F_j,\ \mathrm{A}_{2,j} = -\frac{4\xi}{\xi+1}F_j',\ \mathrm{A}_{3,j} = F_j'',\\
&\mathrm{B}_{1,j} = P_r F_{j+1},\ \mathrm{B}_{2,j} = \frac{n-3}{2}P_r\gamma F_{j+1}F_{j+1}',\ \mathrm{B}_{3,j} = -\frac{\xi+1}{2}P_r\gamma F_{j+1}^2,\\
&R_{1,j} = -\left(1+\frac{1}{\beta_1}\right)F_j''' + \frac{2\xi}{\xi+1}F_j'^2 - F_jF_j'',\\
&R_{2,j} = \left(1+\frac{4}{3}\zeta\right)\theta_j'' + \mathrm{Pr}\,F_j\theta_j' + \gamma\left\{\frac{\xi-3}{2}F_jF_j'\theta_j' - \frac{(\xi+1)}{2}F_j{}^2\theta_j''\right\},
\end{aligned}\right\} \tag{19}$$

We apply the differentiation matrix [D], to the set of Eqns. (9)-(12). This gives:

$$\begin{bmatrix} C_{11} & C_{12} \\ C_{21} & C_{22} \end{bmatrix}\begin{bmatrix} \delta F_j \\ \delta\theta_j \end{bmatrix} = \begin{bmatrix} R_{1,j} \\ R_{2,j} \end{bmatrix} \tag{20}$$

Where

$$\left.\begin{aligned}
&C_{11} = \left(1+\frac{1}{\beta_1}\right)D^3 + \mathrm{A}_{1,j}D^2 + \mathrm{A}_{2,j}D + \mathrm{A}_{3,j}I + \frac{2}{\xi+1}\lambda\theta_j,\ C_{12} = 0,\\
&C_{21} = \left(1+\frac{4}{3}\zeta\right)D^2 + B_{1,j}D,\ C_{22} = +\mathrm{B}_{2,j}D + \mathrm{B}_{3,j}D^2,
\end{aligned}\right\} \tag{21}$$

Here I expresses the identity matrix. Now, the Gauss-Seidel technique can be employed over the above set of matrices to obtain their solutions. All the computations of the above equations are performed in the MATLAB software.

4. Results and discussion

The CSNIS approach is employed to solve the nonlinear differential equations (9)-(12) with the boundary conditions (11)-(12) for the various values of the dimensionless parameters i.e. the mixed convection term λ, the Casson fluid parameter β_1, power-law stretching index ξ, thermal radiation ζ, Prandtl parameter Pr, and the non-Fourier Deborah number γ. We used the following parameters to generate the graphical results for the velocity and temperature profiles: $\mathrm{Pr}=0.72, \lambda=1, \gamma=0.3, \zeta=0.4, \xi=2, \beta_1=1$. Data has been extracted to represent realistic viscoplastic polymers in thermal processing regimes.

Tables 1 and 2 compare the velocity gradient (skin friction) and heat transfer rate (Nusselt number) computed with CSNIS with Vajravelu [39] and Cortell [40]. Setting the following values to zero in the general model i. e. Eqns. (9)-(12) equates the current formulation exactly with the models in [39, 40] which are restricted to *Newtonian viscous flow without mixed convection*: $\beta_1=\infty, \lambda=\zeta=\gamma=0$. It is observed that an excellent agreement has been attained, demonstrating very good accuracy of the CSNIS methodology. Confidence in the CSNIS results is therefore justifiably high. **Table 3** displays the numerical results for skin friction coefficient and Nusselt number for each emerging parameter. In this table, we can observe that the skin friction coefficient decreases as the Casson fluid parameter and mixed convection parameter rise. Conversely both skin friction and Nusselt number are elevated with increasing power law stretching index rises i.e with more intense stretching of the sheet. $\beta_1=\mu_D\sqrt{2\pi_c}/\varsigma$ is the Casson viscoplastic parameter and features in the modified shear term, $\left(1+\frac{1}{\beta_1}\right)F'''$ in the momentum Eqn. (9). As Casson parameter increases the yield stress also increases which inhibits momentum development. This reduces velocity but increases skin friction at the wall. However, the increase in viscoplastic parameter will induce a heating effect in the boundary layer (temperatures will rise) and this will lead to a depletion in heat transferred to the wall. Nusselt numbers are therefore reduced with larger Casson viscoplastic parameter. Generally increasing mixed convection term λ, power-law stretching index ξ, thermal radiation ζ, Prandtl parameter Pr and non-Fourier Deborah number γ all contribute to enhancing Nusselt number magnitudes significantly.

Table 1. Skin friction i. e. wall velocity gradient $F''(0)$ - comparison of CSNIS solutions with earlier special cases where $\beta_1 = \infty, \lambda = \zeta = \gamma = 0$.

ξ	Current Results (CSNIS)	Vajravelu [39] (4th order RK method)	Cortell [40] (RK method)
	$F''(0)$		
1	-1.000000	-1.0000	–1.0000
3	-1.148593	-	-1.1485
5	-1.194487	-1.1944	-
7	1.216850	-	-1.2168
10	-1.234874	-1.2348	–1.2348

Table 2. Nusselt number i. e. wall heat transfer rate $\theta'(0)$ - comparison of CSNIS solutions with earlier special case [34] where $\beta_1 = \infty, \lambda = \zeta = \gamma = 0$.

ξ	Current Results (CSNIS)		Vajravelu [39] (4th order RK method)	
	$\theta'(0)$			
	Pr = 0.71	Pr = 7	Pr = 0.71	Pr = 7
1	–0.458545	–1.895403	–0.4590	–1.8953
5	–0.438819	–1.861581	–0.4394	–1.8610
10	–0.434849	–1.854638	–0.4357	–1.8541

Table 3: Numerical results of skin friction and Nusselt number for all key parameters.

β_1	λ	ξ	ζ	Pr	γ	Skin friction coefficient	Nusselt number
1	1	2	0.4	0.72	0.3	-1.854851	0.851447
2						-1.635221	0.777461
3						-1.549360	0.746962
	1.5					-1.839591	0.858976
	2					-1.822740	0.867202
	3					-1.783062	0.886172
		1.5				-1.618611	0.756410

		2				-1.854851	0.851447
		3				-2.252588	1.046484
			0.2			-	0.803959
			0.3			-	0.828859
			0.5			-	0.872064
				0.71		-	0.843039
				1		-	1.069178
				1.5		-	1.395812
					0.2	-	0.814533
					0.4	-	0.890229
					0.5	-	0.930720

Figs. 2-10 present the velocity and temperature profiles with variation in all control parameters.

The impact of Casson fluid parameter on the profiles of temperature and velocity are illustrated in **Figures 2 and 3**. The velocity is observed to decrease when the Casson fluid parameter is increased, whereas the temperature increases. With increasing Casson fluid parameter i. e. greater viscoplasticity (higher yield stress), the thickness of the momentum boundary layer drops. However back flow is never induced i. e. velocity magnitudes are always positive anywhere in the boundary layer regime transverse to the sheet. However, when the Casson fluid parameter is increased, the thickness of the thermal boundary layer grows. It is noteworthy that asymptotically smooth profiles are computed consistently in the free stream confirming the prescription of an adequately large infinity boundary condition in the CSNIS code.

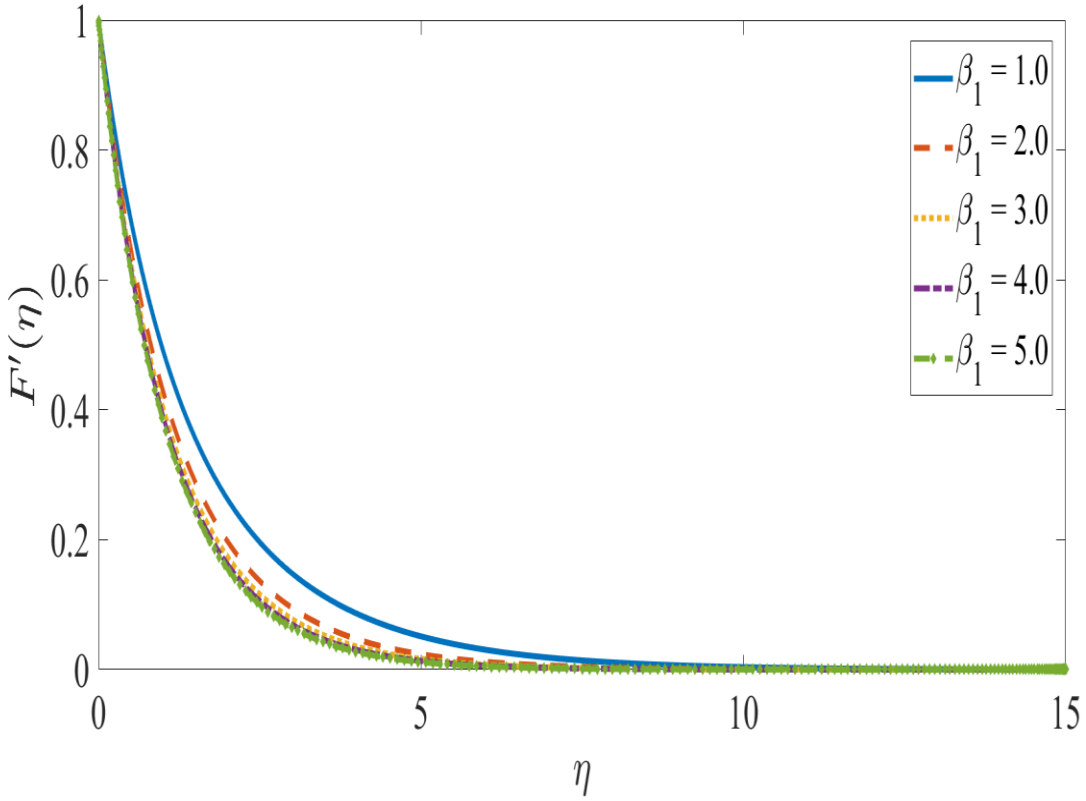

Fig. 2 Influence of β_1 on velocity profiles.

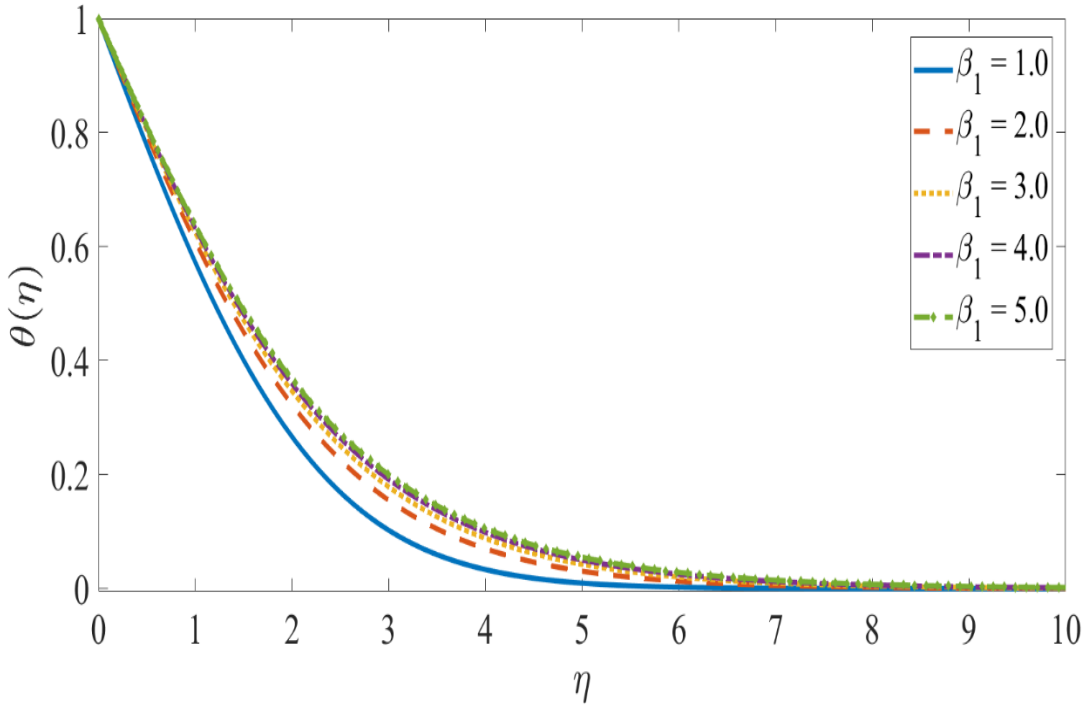

Fig. 3 Influence of β_1 on temperature curves.

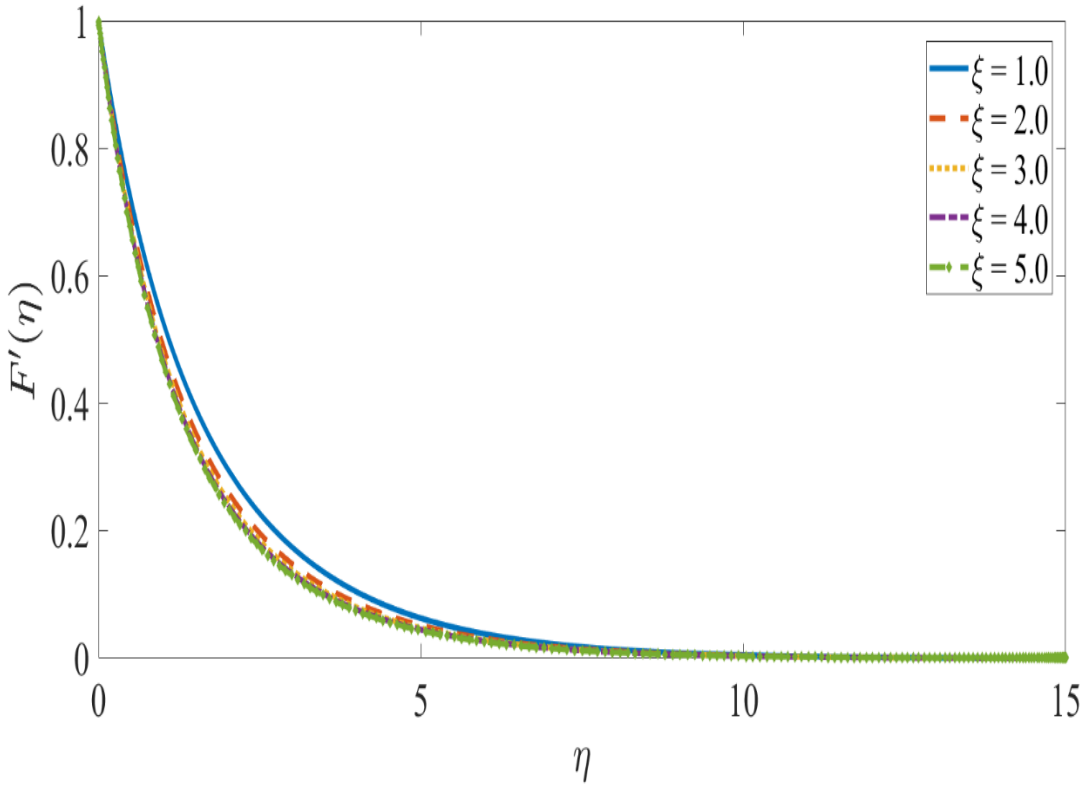

Fig. 4 Influence of ξ on velocity profiles.

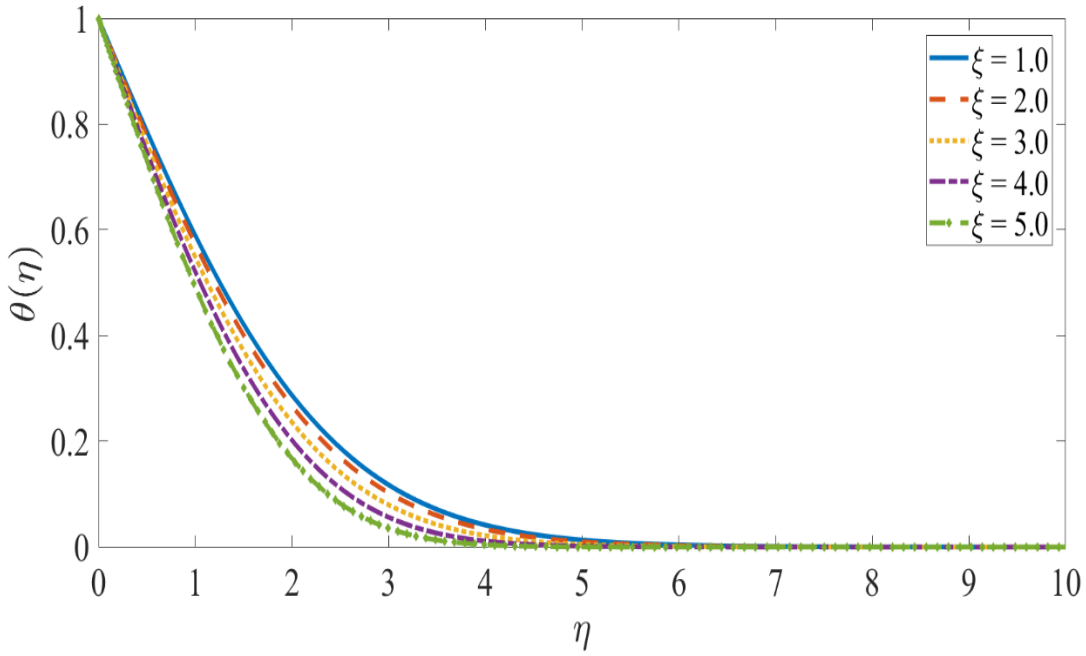

Fig. 5 Influence of ξ on temperature curves.

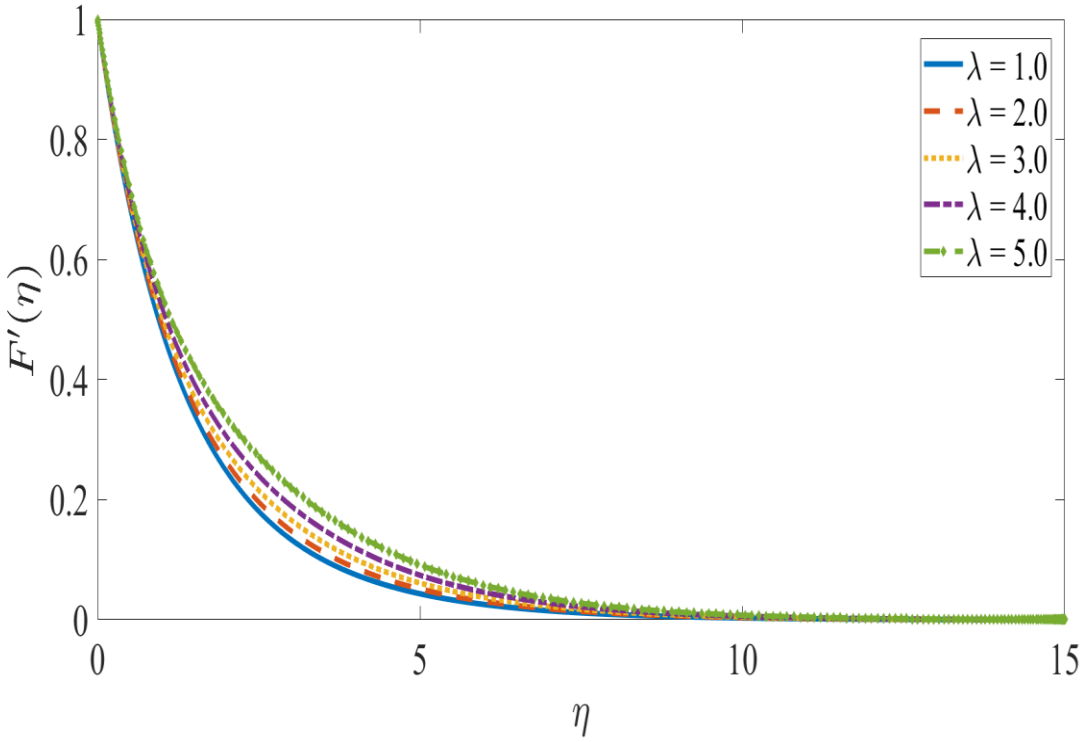

Fig. 6 Influence of λ on velocity profiles.

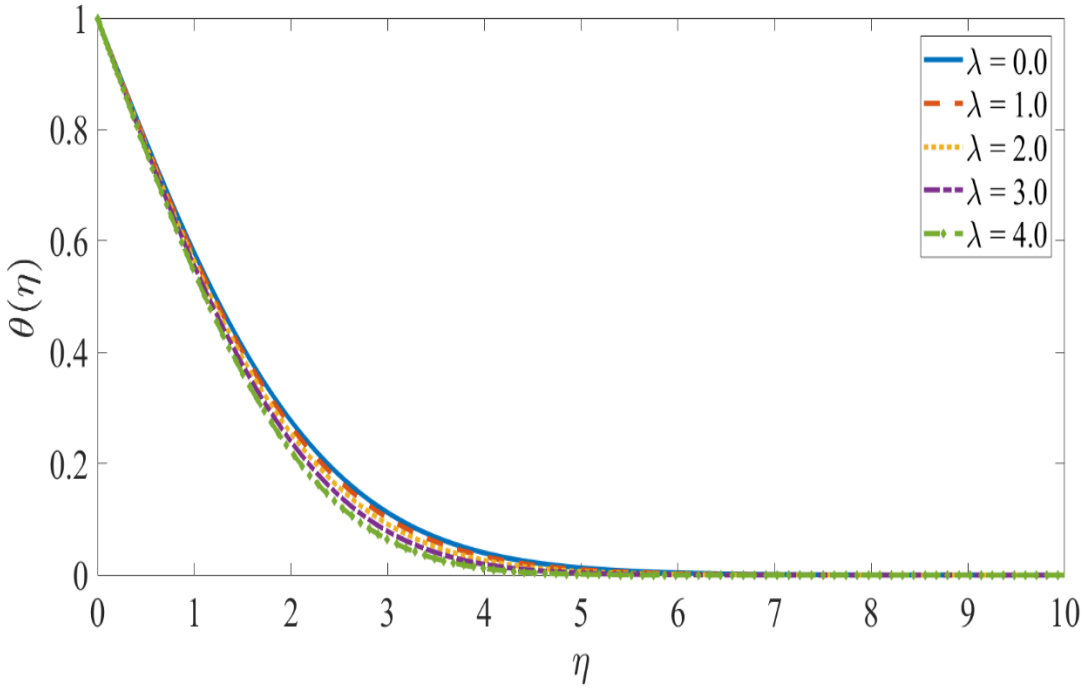

Fig. 7 Influence of λ on temperature distributions.

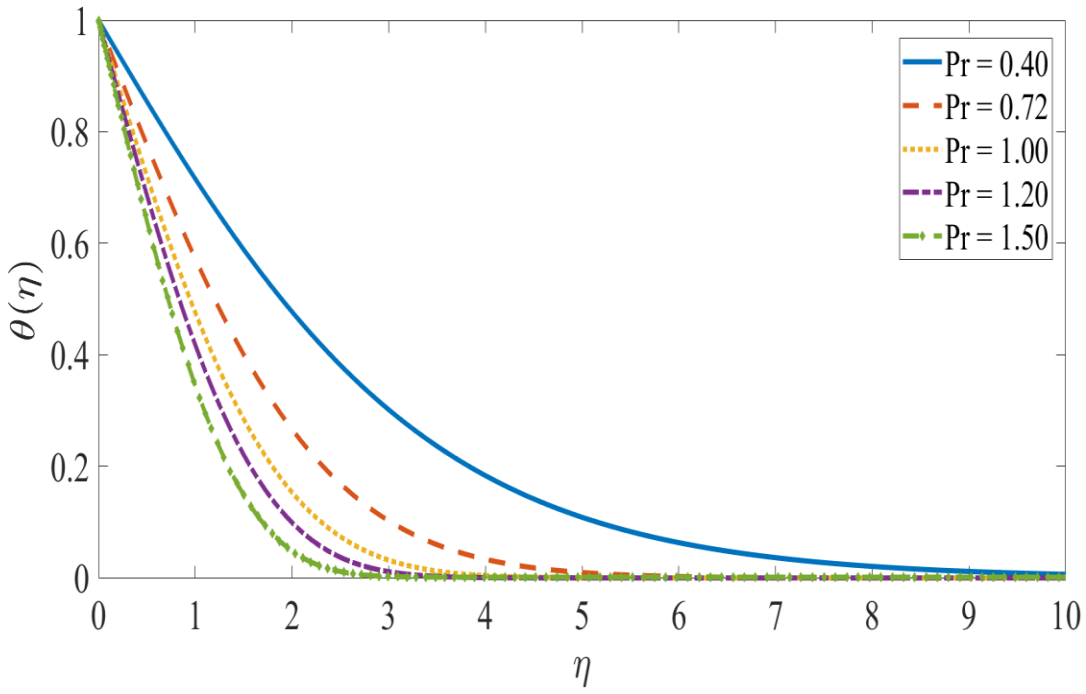

Fig. 8 Impact of Pr on temperature profiles.

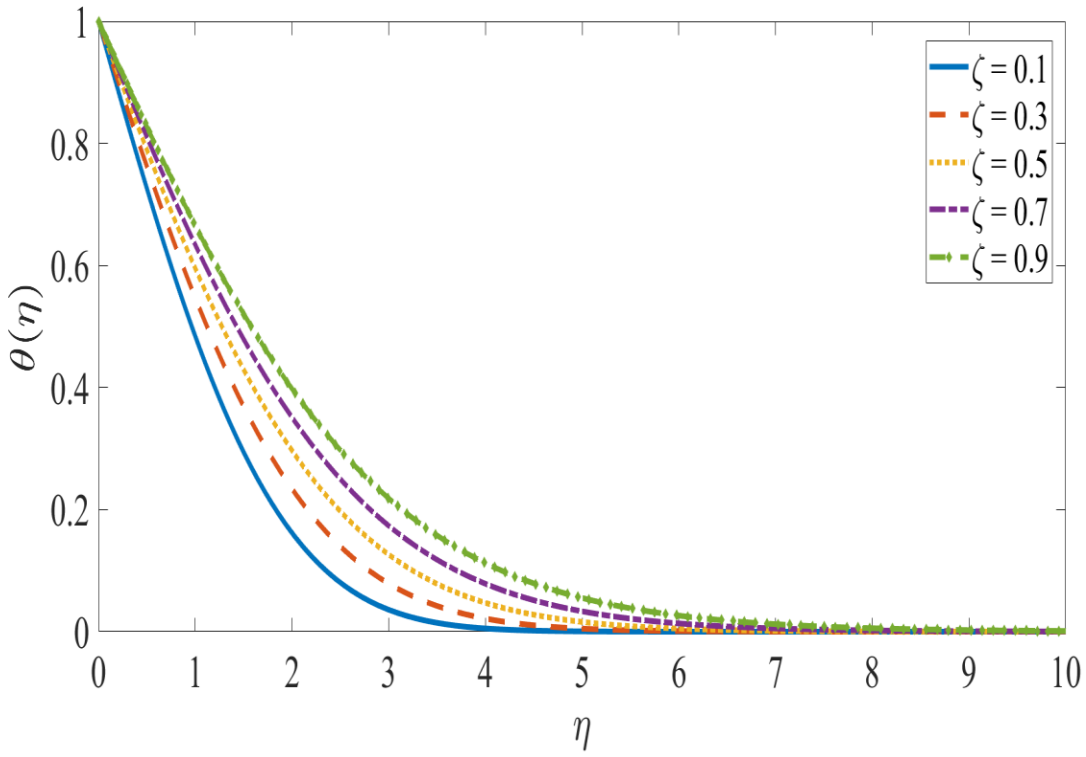

Fig. 9 Impact of ζ on temperature profiles.

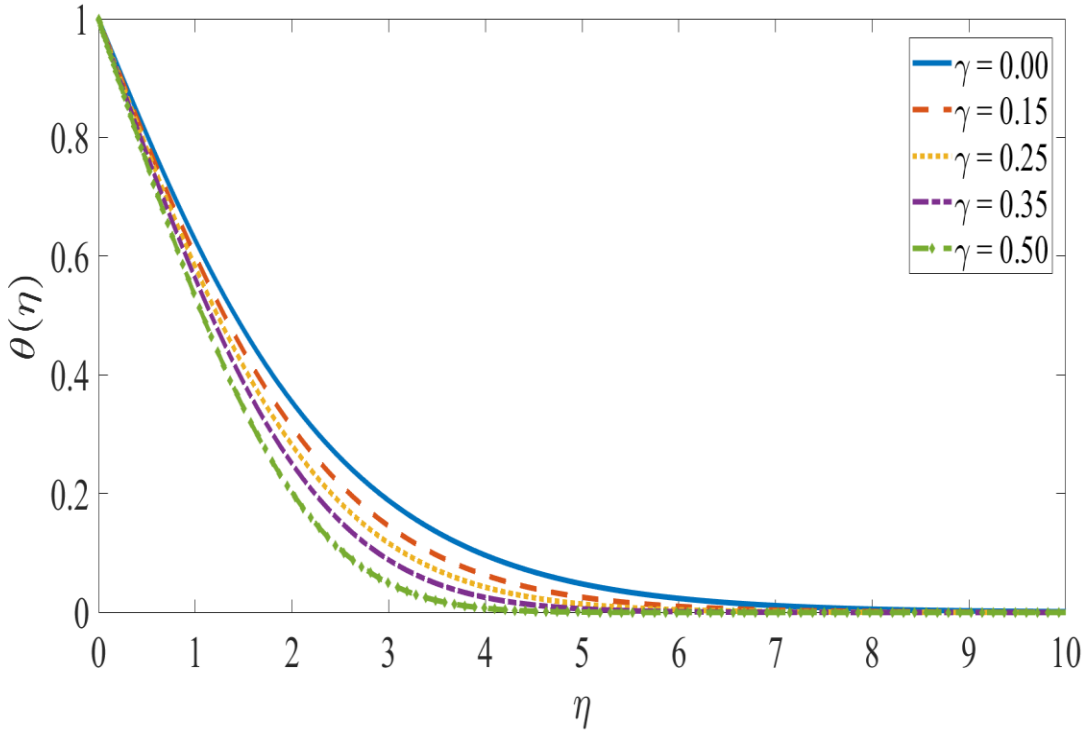

Fig. 10 Influence of γ on temperature curves.

The velocity and temperature profiles with variation in power law stretching index are shown in **Figures 4-5**. It is revealed that when the power index increases, both the fluid velocity and the temperature drop. The basic case of a *linear* elastic stretching surface is retrieved for $\xi = 1$. The parameter, ξ arises in multiple terms in both the momentum and thermal boundary layer Eqns, viz $-\frac{2}{\xi+1}(\xi F'^2 - \lambda\theta)$ in Eqn. (9) and the convective terms, $Pr\,\gamma\left(\frac{\xi-3}{2}FF'\theta' - \frac{\xi+1}{2}F^2\theta''\right)$ in Eqn. (10). By virtue of the definition of the stretching velocity, velocity $U = c\bar{x}^{\xi}$, clearly ξ=2 implies quadratic stretching, ξ=3 corresponds to cubic stretching etc. With increasing stretching rate there is a delay in the momentum imparted to the boundary layer. This suppresses the velocity field and via coupling terms in both equations (9) and (10) also reduces the thermal diffusion, leading to a reduction in temperatures. The case of linear stretching therefore over-predicts both velocity and temperature (and under-predicts momentum boundary layer thickness and over -predicts thermal boundary layer thickness). More realistic results corresponding to actual nonlinear stretching encountered in real polymer processing are therefore only computable with the power-law model.

Figures 6-7 illustrate the effect of the mixed convection term λ on the velocity and temperature distributions. Since the mixed convection term features in the coupling term, $-\frac{2}{\xi+1}(-\lambda\theta)$ which is effectively positive and this exerts a strong effect on the flow characteristics.

When $\lambda = 0$ the case of forced convection is produced. Higher values of $\lambda = \frac{Gr}{\Re^2} = \frac{\frac{g\beta(T_W - T_\infty)\bar{x}^3}{\nu^2}}{\frac{U^2\bar{x}^2}{\nu^2}}$ imply a boost in Grashof number and accentuation in thermal buoyancy force relative to viscous force. This will accelerate the boundary layer flow whereas it will inhibit thermal diffusion in the regime. Both momentum boundary layer thickness and thermal boundary layer thickness will be reduced.

Figure 8 depicts the influence of the Prandtl number Pr on the thermal profile. A sharp decrement in temperature is induced with larger Prandtl number. As *Pr* increases, the thickness of the thermal boundary layer decreases. The momentum-to-thermal diffusivity ratio is expressed by the Prandtl number. Prandtl number also expresses the ratio of momentum to thermal boundary layer thickness. When Pr =1 both momentum and energy diffuse at the same rate and the boundary layer thicknesses are equal. Prandtl number is also inversely proportional to thermal conductivity. Higher *Pr* therefore implies a reduction in polymer thermal conductivity which manifests in a reduction in temperatures. Since lower Prandtl liquids have greater thermal conductivities than higher liquids, heat may permeate from the sheet more rapidly. As a consequence, Prandtl number choice (depending on the polymer utilized) may be exploited to accelerate cooling.

Figure 9 demonstrates how temperature distribution is modified with thermal radiation parameter, ζ The radiative flux energizes the polymeric flow. $\zeta = \frac{4\bar{\sigma}{T_\infty}^3}{k^*\kappa}$ and expresses the relative contribution of *thermal radiation to thermal conduction* in the regime. When $\zeta = 0$, radiative flux vanishes from the augmented thermal diffusion term, $\left(1 + \frac{4}{3}\zeta\right)\theta''$ in Eqn. (10), and temperature and thermal boundary layer thickness are minimized. With increment in thermal radiation parameter, thermal diffusion is exacerbated in the boundary layer which produces a boost in temperatures. It is also noteworthy that when $\zeta = 1$, b*oth thermal conduction and thermal radiation contribute equally* whereas when $\zeta < 1$, thermal conduction is dominant.

Figure 10 shows that at higher values of the non-Fourier Deborah number γ , a considerable decrease in temperatures inside the boundary layer is induced. There will also be a corresponding reduction in the thickness of the thermal boundary layer. In the non-Fourier model, the modified Deborah number features the supplemental impact brought on by thermal relaxation time. By setting $\gamma = 0$, the Cattaneo-Christov heat flux model (non-Fourier), is reduced to the classical Fourier model. $\gamma = \lambda_2 c\bar{x}^{\xi-1}$ and features in the modified thermal diffusion terms, $+Pr\,\gamma\left(\frac{\xi-3}{2}FF'\theta' - \frac{\xi+1}{2}F^2\theta''\right)$ in Eqn. (9). Higher thermal relaxation effect implies a longer time required for thermal waves to propagate in the polymer and results in a cooling effect i. e. decrease in temperature. Lower thermal relaxation corresponds to a faster propagation of thermal waves which produces higher temperatures. Evidently the inclusion of

thermal relaxation i. e. non-Fourier effects avoids the over-prediction of temperature encountered with the classical Fourier model.

5. Concluding Remarks

Motivated by simulating thermal non-Newtonian polymer coating flows, in this article the laminar viscoplastic boundary layer flow and mixed convective heat transfer over a power-law nonlinear stretching surface with thermal relaxation effects has been studied. The hyperbolic Cattaneo-Christov heat flux model has been used. The non-Newtonian polymer characteristics are described by employing the Casson flow model. The Rosseland diffusion flux model has been employed for thermal radiation. Via robust similarity transformations, the primitive partial differential conservation equations for momentum and energy equations have been converted into a system of coupled non-linear ordinary differential equations with associated wall and free stream boundary conditions. A Chebyshev Spectral Newton Iterative scheme (CSNIS) in the MATLAB platform has been implemented to solve the nonlinear boundary value problem. Verification of the method has been achieved via comparisons with Newtonian flow and classical Fourier heat flux solutions presented in the literature. The main findings of the present computations can be summarized as follows:

1. When the Casson viscoplastic fluid parameter is increased, the fluid velocity is depleted whereas temperature magnitudes are increased.
2. When the mixed convection parameter is enhanced, the flow is accelerated strongly whereas temperature is reduced substantially.
3. The temperature and fluid velocity both decline as the power law stretching index parameter is enhanced.
4. An elevation in the Prandtl number reduces the thickness of the thermal boundary layer and suppresses temperatures, whereas temperature is strongly boosted with increment in thermal radiation parameter.
5. Higher non-Fourier Deborah numbers induce a reduction in thermal boundary layer thickness as well as a considerable decrease in temperature profile due to larger thermal relaxation times.
6. Nusselt number is strongly boosted with increasing mixed convection parameter, radiative parameter, Prandtl number and non-Fourier Deborah number

CSNIS has been shown to hold significant promise in numerical analysis of nonlinear rheological thermal polymer coating flows. Attention has however been restricted to a viscoplastic model. Future investigations may consider viscoelastic polymers and utilize for example the FENE-P model. Efforts in this direction will be communicated imminently [44].

References

[1] Hsiao K L., Conjugate heat transfer of magnetic mixed convection with radiative and viscous dissipation effects for second-grade viscoelastic fluid past a stretching sheet. 2007. *Appl. Thermal Engng.* 27(11-12): 1895-1903.

[2] Mukhopadhyay S. Heat transfer analysis of the unsteady flow of a Maxwell fluid over a stretching surface in the presence of a heat source/sink. 2012. *Chin. Phys. Lett*. 29: 054703.

[3] Mukhopadhyay S and Bhattacharyya K. Unsteady flow of a Maxwell fluid over a stretching. surface in presence of chemical reaction. 2012. *J. Egyptian Math. Society* 20(3): 229-234.

[4] Mukhopadhyay S. Upper-Convected Maxwell fluid flow over an unsteady stretching surface embedded in porous medium subjected to suction/blowing. 2012. *Z. Naturforsch*. (67a): 641-646.

[5] Y. Jaluria, Heat and mass transfer in the extrusion of non-Newtonian materials. *Adv. Heat Tran.* 28, 145–230 (1996).

[6] J. Prakash, Dharmendra Tripathi, Nevzat Akkurt and O. Anwar Bég, Tangent hyperbolic non-newtonian radiative bioconvection nanofluid flow from a bi-directional stretching surface with electro-magneto-hydrodynamic, Joule heating and modified diffusion effects, *European Physical Journal Plus (Italy).* (2022) 137: 472 (22 pages) doi.org/10.1140/epjp/s13360-022-02613-x

[7] M. Kumar, G. J. Reddy, N. N. Kumar and O. Anwar Bég, Application of differential transform method to unsteady free convective heat transfer of a couple stress fluid over a stretching sheet, *Heat Transfer,* 48, 582-560 (2019).

[8] Kumar K.A. Sugunamma V. Sandeep N. Numerical exploration of MHD radiative micropolar liquid flow driven by stretching sheet with primary slip: a comparative study, *J. Non-Equilibrium Thermodyn.* 2019. 44(2): 101e122.

[9] Kumar K.A. Sugunamma V. Sandeep N. Impact of non-linear radiation on MHD non-aligned stagnation point flow of micropolar fluid over a convective surface, *J. Non-Equilibrium Thermodyn*. 2018. 43 (4): 327e345.

[10] Megahed A.M. Flow and heat transfer of non-Newtonian Sisko fluid past a nonlinearly stretching sheet with heat generation and viscous dissipation, *J. Brazilian Soc. Mechani. Scie. and Eng.* 2018. 40(10): 492.

[11] S. Han and J.Peddieson, Non-Fourier heat conduction/convection in moving medium, *International Journal of Thermal Sciences*, 2018, 130, 128-139.

[12] Cattaneo C. Sulla conduzione del calore. *Atti Semin. Mat Fis Univ Modena Reggio Emilia* 1948; 3: 83–101. 24.

[13] Christov CI. On frame indifferent formulation of the Maxwell–Cattaneo model of finite-speed heat conduction. *Mech Res Commun* 2009; 36: 481–486.

[14] G. Kumaran, R Sivaraj, V. Ramachandra Prasad, O. Anwar Bég, Numerical study of axisymmetric magneto-gyrotactic bioconvection in non-Fourier tangent hyperbolic nano-functional reactive coating flow of a cylindrical body in porous media, *European Physical Journal Plus, 136, 1107 (2021). https://doi.org/10.1140/epjp/s13360-021-02099-z (32 pages).*

[15] A. Shahid, M. M. Bhatti, O. Anwar Bég and A. Kadir, Numerical study of radiative Maxwell viscoelastic magnetized flow from a stretching permeable sheet with the Cattaneo–Christov heat flux model, *Neural Computing and Applications,* 30, 3467–3478 (2018).

[16] A. Alhowaity *et al.,* Non-Fourier energy transmission in power-law hybrid nanofluid flow over a moving sheet**,** *Scientific Reports***,** 12, Article number: 10406 (2022)**.**

[17] Rashid Mehmood, S. Rana, O. Anwar Bég and A. Kadir, Numerical study of chemical reaction effects in magnetohydrodynamic Oldroyd-B oblique stagnation flow with a non-Fourier heat flux model, *J. Brazilian Soc. Mech Sci. Eng.* 40:526-*539 (2018).*

[18] Sui, J., Zheng, L. & Zhang, X. Boundary layer heat and mass transfer with Cattaneo-Christov double-diffusion in upper-convected Maxwell nanofluid past a stretching sheet with slip velocity. *Int. J. Therm. Sci.* 104, 461–468 (2016).

[19] Han S.H. Zheng L.C. Li C.R. Zhang X.X. Coupled flow and heat transfer in visco-elastic fluid with Cattaneo-Christov heat flux model, *Appl. Math Letters*. 2014. 38: 87e93.

[20] Mustafa M. Cattaneo-Christov heat flux model for rotating flow and heat transfer of upper convected Maxwell fluid, *AIP Adv*. 2015. 5: 047109.

[21] Kumar K.A. Ramana Reddy J.V. Sugunamma V. Sandeep N. Magnetohydrodynamic Cattaneo-Christov flow past a cone and a wedge with variable heat source/sink, *Alex. Eng. J.* 2018. 57: 435e443.

[22] M. Saqlain *et al.,* Transportation of heat and mass of nonlinear mixed convective boundary flow of Casson fluid with generalized Fourier's and Fick's laws and stratification effect, *Proc IMechE Part C: J Mechanical Engineering Science IMechE* 2021 DOI: 10.1177/09544062211039531 2022, Vol. 236(7) 3387–3397.

[23] M. M. Bhatti, A. Shahid, Ioannis E. Sarris and O. Anwar Bég, Spectral relaxation computation of Maxwell fluid flow from a stretching surface with quadratic convection and non-Fourier heat flux using Lie symmetry transformations, *International Journal of Modern Physics B, 2350082 (2022 pages) DOI: 10.1142/S0217979223500820 (21 pages)*

[24] S.R. Mishra, M. Shamshuddin, O. Anwar Bég, Ali Kadir, Numerical study of heat transfer and viscous flow in a dual rotating extendable disk system with a non-Fourier heat flux model, *Heat Transfer*, 48 (1), 435-459 (2019).

[25] Atul Kumar Ray, B. Vasu, P. V. S. N. Murthy, O. Anwar Bég, R.S.R. Gorla and B. Kumar, Convective flow of non-homogeneous rheological nanofluids with non-Fourier thermal relaxation -application in polymer coating, *Arabian J. Science Engineering (2021).* https://doi.org/10.1007/ s13369-021-06467-w (18 pages)

[26] R.L. Batra and A. Kandasamy, Entrance region flow of a Casson fluid in a straight channel, *Polymer-Plastics Technology and Engineering*, 31, 527-554 (1992).

[27] Chhabra, R.P., Richardson,J.F.: *Non-Newtonian Flow in Process Industries*. Butterworth-Heinemann, Oxford, UK (1999).

[28] Ullah I, Alkanhal TA, Shafie S, et al. MHD slip flow of Casson fluid along a nonlinear

permeable stretching cylinder saturated in a porous medium with chemical reaction, viscous dissipation, and heat generation/ absorption. *Symmetry* 2019; 11: 531

[29] J. Richeton, S. Ahzi, K. Vecchio, F. Jiang, R. Adharapurapu, Influence of temperature and strain rate on the mechanical behavior of three amorphous polymers: Characterization and modeling of the compressive yield stress, *International Journal of Solids and Structures* 43 (2006) 2318–2335.

[30] V. Rao, Radiation processing of polymers, *Advances in Polymer Processing: From Macro- to Nano- Scales*, 2009, Pages 402-437

[31] M.M. Bhatti, C.M. Khalique, Tasveer Bég, O. Anwar Bég and Ali Kadir, Numerical study of slip and radiative effects on magnetic Fe_3O_4-water-based nanofluid flow from a nonlinear stretching sheet in porous media with Soret and Dufour diffusion, *Modern Physics Letters B 33*, 2050026 (24 pages) (2020).

[32] Siva Reddy Sheri, O. Anwar Bég, P. Modugula *and* A. Kadir, Computation of transient radiative reactive thermo-solutal magneto-hydrodynamic convection in inclined MHD Hall generator flow with dissipation and cross diffusion, *Computational Thermal Sciences*, 11 (6) 541-563 (2019).

[33] Mahmood A. Chen B. Ghaffari A. Hydromagnetic Hiemenz flow of micropolar fluid over a nonlinearly stretching/shrinking sheet: Dual solutions by using Chebyshev Spectral Newton Iterative Scheme, *Journal of Magnetism and Magnetic Materials*. 2016. (416): 329-334.

[34] Abouelregal, A. E., & Marin, M. (2020). The size-dependent thermoelastic vibrations of nanobeams subjected to harmonic excitation and rectified sine wave heating. *Mathematics*, *8*(7), 1128. https://doi.org/10.3390/math8071128

[35] Scutaru, M. L., Vlase, S., Marin, M., & Modrea, A. (2020). New analytical method based on dynamic response of planar mechanical elastic systems. *Boundary Value Problems*, *2020*(1). https://doi.org/10.1186/s13661-020-01401-9

[36] Animasaun, I. L., Kumar, T. K., Noah, F. A., Okoya, S. S., Al-Mdallal, Q. M., & Bhatti, M. M. (2022). Insight into Darcy flow of ternary-hybrid nanofluid on horizontal surfaces: Exploration of the effects of convective and unsteady acceleration. *Zeitschrift Fur Angewandte Mathematik Und Mechanik*. https://doi.org/10.1002/zamm.202200197

[37] Zhang, L., Bhatti, M. M., Bég, O. A., Leonard, H. J., & Kuharat, S. (2022). Numerical study of natural convection dissipative electro-magnetic non-Newtonian flow through a non-Darcy channel. *Zeitschrift Fur Angewandte Mathematik Und Mechanik*, *102*(10). https://doi.org/10.1002/zamm.202100608

[38] Bhatti, M. M., & Ellahi, R. (2023). Numerical investigation of non-Darcian nanofluid flow across a stretchy elastic medium with velocity and thermal slips. *Numerical Heat Transfer, Part B: Fundamentals*, 1-21. https://doi.org/10.1080/10407790.2023.2174624

[39] K. Vajravelu, Viscous flow over a nonlinearly stretching sheet, Appl. Math. Comput. 124(3) (2001) 281–8. 10.1016/s0096-3003(00)00062-x.

[40] R. Cortell, Viscous flow and heat transfer over a nonlinearly stretching sheet, *Appl. Math. Comput*. 184(2) (2007) 864–73. 10.1016/j.amc.2006.06.077.
[41] Majeed A. Javed T. Ghaffari A. Rashidi M.M. Analysis of heat transfer due to stretching cylinder with partial slip and prescribed heat flux: a Chebyshev spectral Newton iterative scheme, *Alexandria Eng. J.* 2015. 54(4): 1029-1036.
[42] Motsa, S. S. A new spectral local linearization method for nonlinear boundary layer flow problems, *Journal of Applied Mathematics*, 2013. Article ID 423628.
[43] Trefethen LN. *Spectral methods in MATLAB*, volume 10 of Software, Environments, and Tools. Society for Industrial and Applied Mathematics (SIAM), Philadelphia, PA. 2000; 24.
[44] M. Norouzi. S. Z. Daghighi. O. Anwar Bég Exact analysis of heat convection of viscoelastic FENE-P fluids through isothermal slits and tubes, *Meccanica,* 53, 817-831 (2018).